The Journal of Energy: Engineering & Management
Vol. 10, No. 4, Winter 2021, P. 60-73

[DOR: 20.1001.1.23452951.1399.10.4.3.5]
[DOI: 10.22052.10.4.60]

A New Control Strategy for Controlling Isolated Microgrid

F. Amiri[1], M.H. Moradi[2*]

[1] Department of Electrical Engineering, Bu-Ali Sina University, Hamedan, I.R.Iran
f.amiri94@basu.ac.ir
[2] Department of Electrical Engineering, Bu-Ali Sina University, Hamedan, I.R.Iran
mh_moradi@yahoo.co.uk

Abstract

Microgrid control in the isolated mode is a highly important subject area. In the present paper, a new method is used for controlling isolated microgrids. This method was used based on the classification of the microgrids into two groups, namely fast-dynamic (battery and flywheel) and slow-dynamic (diesel generator, electrolyzer, and fuel cell). For the microgrid components with fast dynamics, a separate controller has been used. Also, another separate controller has been deployed for those components of the microgrid that are characterized by slow dynamics. This method was simulated in MATLAB software. A fractional-order proportional-integral-differential (FOPID) controller optimized by the grey wolf optimizer (GWO) algorithm was used as the proposed controller in the new control strategy. The proposed method was compared with the FOPID controller that has been optimized by particle swarm optimization (PSO) algorithm and genetic algorithm (GA). Besides, it was compared with the common Proportional-Integral-Differential (PID) controller, the coefficients of which have been obtained using the *Ziegler-Nichols* method, and proportional-integral (PI) controller, the coefficients of which have been obtained using the neural network (NN) method. The obtained results indicated the improved response speed, improved transient-state performance, and an improved steady-state performance of the proposed method compared with those mentioned.

Keywords: Isolated Microgrid, New Control Strategy, Fractional Order PID Controller, Grey Wolf Optimize.

* Corresponding Author

[DOR: 20.1001.1.23452951.1399.10.4.3.5]

[DOI: 10.22052.10.4.60]

1. Introduction

The occurrence of distributed generation resources results in several problems, including: the preservation and protection of resources; resources' method of participation in regulating main parameters such as frequency, voltage; the process of power exchange between the global network and the distributed generation resources, and so on. to resolve these issues and to give an integrated and unified consideration to these resources and local loads, the Consortium for Electric Reliability Technology Solutions (CERTS) introduced the concept of Microgrids (MG) for the first time in modern power systems by in 1998. According to this introduction, microgrids are small power networks comprised of several distributed generation resources and local loads. Microgrids are normally connected to the global network, and in case of an emergency, based on the occurrence of heavy disturbances, they become disconnected from the global network and can solely feed major and important local loads [1]. Microgrids can be connected to the power network or disconnected from it, but controlling a microgrid in an isolated state is of greater importance [2]. Microgrid components involve different dynamics, and, an effective control, by using the proposed control strategy, can be achieved in isolated microgrids [3]. If a disturbance occurs in the power system and disrupts the balance between production and consumption, the frequency will fluctuate. For example, if a load is suddenly added, frequency will decline from the rated value which, if not controlled, leads to frequency instability. The primary control loop is the first control loop that attempts to limit frequency decline after the occurrence of a disturbance. The primary control loop limits the declined frequency. However it is incapable of restoring frequency to its rated value, so another interactive loop known as the secondary frequency control is also utilized which, with the occurrence of disturbances, restores frequency to its rated value [4-6]. Various controllers are used to reduce frequency fluctuations in microgrids. One of them is the Proportional-Integral-Differential (PID) controller, the coefficients of which have been obtained through the Ziegler-Nichols method. In this method, for each controllable microgrid component, the PID controller - the coefficients of which have been obtained through the Ziegler-Nichols method - is used to control the frequency of isolated microgrids [7]. The particle swarm algorithm method has been used to optimize PID controller coefficients for each of the controllable components in order to reduce frequency fluctuations in isolated microgrids [8]. In [9,10] have also used a secondary frequency control on renewable energy sources convertors for load-frequency control. In [11-13], robust controller methods have been used to design the controller such that [11,12] have presented the H-infinity (H∞) control and in [13], a progression algorithm based on robust control using μ-synthesis and D-K iteration method (D-K) has been presented. In [14-18], the Droop Control method (linear droop control in [14-16], non-linear droop control in [17], and linear droop control along with controllable loads in [18]) has been presented to load-frequency control in the microgrid. In [19], an observer-based sliding mode control has been used to control the frequency-load in the microgrid. Among metaheuristic algorithm-based controllers, instances such as Genetic Algorithm (GA) in [20], Particle Swarm Optimization (PSO) algorithm in [21], Social-Spider Optimizer (SSO) algorithm in [22], Biogeography-Based Optimization (BBO) algorithm in [23] for regulating PID, and Enhanced Harmony Search Algorithm in [24] can be mentioned for controlling load-frequency in microgrids. In [25-27], fuzzy controllers, the coefficients of which have been determined by the Particle Swarm algorithm in [25] and type-2 fuzzy logic in [26, 27] have been used for controlling load-frequency. Each of the above-mentioned methods has problems regarding response speed and high fluctuations in the event of disturbances in an isolated microgrid.

A novel control strategy has been utilized in this paper for controlling an isolated microgrid. Firstly, linear microgrid modelling was implemented using a controller to determine whether each of the microgrid components is of fast or slow dynamics. A Fractional Order Proportional Integral Differential (FOPID) controller was used for fast dynamic microgrid components followed by a Fractional Order Proportional Integral Differential controller for slow dynamic components. The Grey Wolf

[DOR: 20.1001.1.23452951.1399.10.4.3.5]
[DOI: 10.22052.10.4.60]

algorithm was used for optimizing the controller coefficients of each microgrid component (slow dynamic and fast dynamic). Among the advantages of the proposed control strategy in comparison with conventional methods are more optimal transient responses, steady responses, and response speed. In the proposed control strategy, the coefficients of fast dynamic controllers play a role in the transient system response, and the coefficients of slow dynamic controllers impact the steady system response. Indeed, slow dynamic component controllers are influential on the transient response, but their impact is far less than that of fast dynamic component controllers. Also, fast dynamic component controllers are effective on steady responses, but their impact is far less than that of slow dynamic component controllers. This article consists of several sections which in sequence are: microgrid and its components, a dynamic model, a proposed control strategy, simulation, and a conclusion.

2. Microgrid and its Components

The studied microgrid consists of solar cells, wind turbine, diesel generator, fuel cell, electrolyzer, battery, flywheel, load, and a controller. The dynamic model of microgrid is illustrated in Fig. 1.

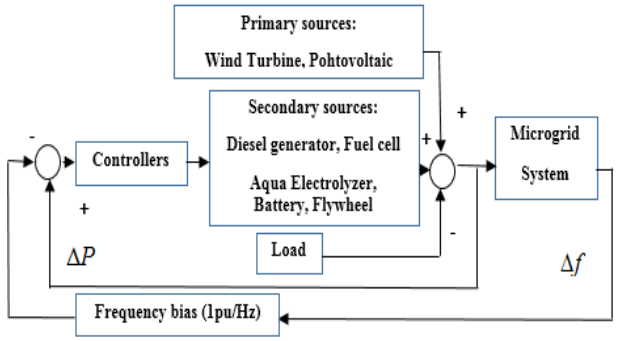

Fig. 1: The Dynamic model of a microgrid

2. 1. Diesel Generator (DG)

Diesel Generator (DG) has a major role in the independent hybrid microgrid. It supplies power deficit in order to achieve a state of balance. Power deficit is supplied through the mechanisms of power and speed control. The diesel generator system is depicted via (1) [8].

$$G_{DG}(s) = \frac{k_{DG}}{1 + sT_{DG}} \quad (1)$$

T_{DG}, k_{DG} are the diesel generator time constant and gain respectively. Its transfer function is depicted via (2) [8].

$$G_D(s) = \frac{k_D}{1 + sT_D} \quad (2)$$

T_D, k_D are the diesel generator time constant and gain respectively, when a delay is considered for the diesel generator output. Therefore, the diesel generator system is depicted via (3) [8].

$$G_{DEG}(s) = G_D(s)G_{DG}(s) = \frac{k_{DG}}{1+sT_{DG}} * \frac{k_D}{1+sT_D} \quad (3)$$

The power of the diesel generator is between 0-0.8 per unit. The dynamic model of diesel generator is illustrated in Fig. 2.

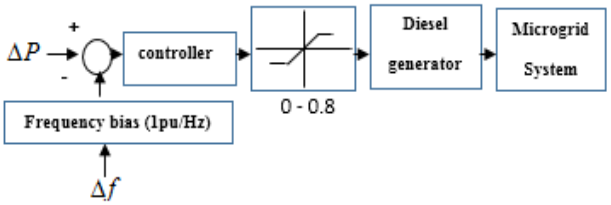

Fig. 2: The dynamic model of diesel generator

2. 2. Aqua Electrolyzer (AE)

The electrolyzer helps absorb system fluctuations quickly. The electrolyzer gains power from the system and produces hydrogen through electrolysis which is used as fuel in the fuel cell for production. The electrolyzer transfer function is presented in (4) [1,7].

$$G_{AE} = \frac{k_{AE}}{1 + sT_{AE}} \quad (4)$$

k_{AE}, T_{AE} are electrolyzer gain and time constant respectively. The limitation of power absorbed by the electrolyzer is between 0-0.2 per unit. The dynamic model of electrolyzer, with the consideration of delay, is illustrated in Fig. 3.

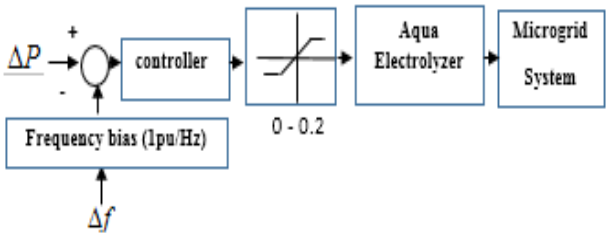

Fig. 3: The dynamic model of electrolyzer

2. 3. Fuel Cell (FC)

The fuel cell is a device that converts chemical energy to electrical energy. The fuel cell requires a

constant source of fuel and oxygen for chemical reactions. Among the advantages of the fuel cell is the constant and steady production of electricity, as long as the input is available, and low contamination and high efficiency. The fuel cell model is presented in (5) [1,7].

$$G_{FC}(s)=\frac{k_{FC}}{1+sT_{FC}} \quad (5)$$

k_{FC}, T_{FC} are fuel cell gain and time constant respectively. The output power limitation of the fuel cell is between 0-0.3 per unit. The dynamic model of fuel cell's, with the consideration of delay, is illustrated in Fig. 4.

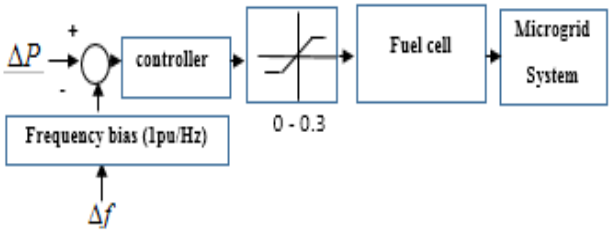

Fig. 4: The dynamic model of fuel cell

2. 4. Battery Energy Storage System (BESS)

A battery is an electro-chemical device that converts chemical energy to electrical energy. Batteries enhance the dynamic and transient stability of renewable energy sources. Batteries are capable of storing the energy produced by renewable sources and retrieving them when necessary. The battery transfer function is presented in (6) [1,7].

$$G_{BESS}(s)=\frac{k_{BESS}}{1+sT_{BESS}} \quad (6)$$

k_{BESS}, T_{BESS} are battery gain and battery time constant respectively. Charging and discharging limitations of the battery is between -0.5,0.5 per unit. Fig. 5 illustrates the battery's dynamic model, with the consideration of delay.

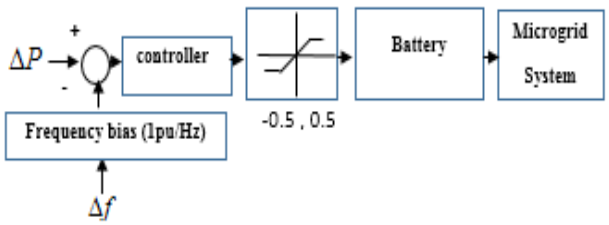

Fig. 5: The dynamic model of Battery

2. 5. Flywheel Energy Storage System (FESS)

The energy stored in the flywheel energy storage system is in the form of kinetic energy stored in the flywheel. Equation (7) is the defined kinetic energy [7].

$$k_E=\frac{1}{2}IW^2 \quad (7)$$

I : is the moment of flywheel inertia (N-m-sec^2)

W : is the angular frequency deviation (rad/s)

The flywheel energy storage system model has been defined via (8).

$$G_{FESS}(s)=\frac{k_{FESS}}{1+sT_{FESS}} \quad (8)$$

T_{FESS}, k_{FESS} are flywheel time constant and flywheel gain respectively. The power limitations of flywheel energy storage system are considered between -0.5,0.5 per unit. The dynamic model of flywheel is illustrated in Fig. 6.

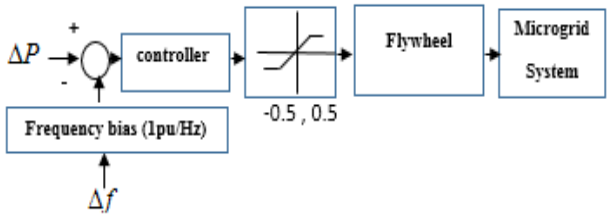

Fig. 6: The dynamic model of flywheel

3. 6. Solar Photovoltaic

By series and parallel connection of solar photovoltaic cells, higher voltages and currents can be achieved. The output power of the solar photovoltaic cell is depicted via (9) [1,8].

$$P_{SPV}=\eta S\varphi[1-.005(T_a+25)] \quad (9)$$

η : Solar Photovoltaic efficiency

S : Solar Photovoltaic area (m^2)

ϕ : Radiation (kw/m^2)

T_a : Environment temperature (deg.cel)

The solar photovoltaic cell is dependent on T_a and ϕ, while η and S are constant. In this paper, environmental temperature has been considered invariable, and P_{SPV} changes linearly with ϕ. The solar photovoltaic model has been depicted via (10), where k_{SPV} and T_{SPV} are the gain and time constant of the solar photovoltaic respectively.

$$G_{SPV}(s)=\frac{k_{SPV}}{1+sT_{SPV}} \quad (10)$$

2. 7. Wind Turbine Generator (WTG)

The wind turbine model is depicted via (11), where

[DOR: 20.1001.1.23452951.1399.10.4.3.5]
[DOI: 10.22052.10.4.60]

k_{WTG} and T_{WTG} are the gain and time constant of the wind turbine generator respectively [22,23].

$$G_{WTG}(s)=\frac{k_{WTG}}{1+sT_{WTG}} \quad (11)$$

2. 8. Power and Frequency Deviation

To maintain the microgrid at a steady function, the frequency-power balance must be sustained; Such balance can be achieved by controlling the various components of the microgrid. The exchanged power is depicted via (12).

$$\Delta P = P_s - P_L \quad (12)$$

P_s: Total production capacity of microgrid

P_L: Power of Load

Power variations in the microgrid will lead to frequency deviations. Microgrid frequency variations are depicted via (13).

$$\Delta F = \frac{\Delta P}{k_{SYS}} \quad (13)$$

k_{SYS} : Frequency constant of microgrid

ΔF : Frequency deviations of microgrid

ΔP : Power deviations

In practice, a delay occurs between system power deviation and frequency deviation, which is shown as (14) [22,23].

$$G_{SYS}(s)=\frac{1}{k_{SYS}(1+sT_{SYS})}=\frac{1}{D+sM} \quad (14)$$

M: Inertia constant

D: System damping

3. Microgrid Linear Model

Firstly, according to Fig. 1 and data of Table 1, microgrid linear equations have been obtained based on (15). Microgrid components include solar cells, wind turbine, diesel generator, electrolyzer, fuel cell, battery, flywheel, load, and a controller. The microgrid linear model is depicted in (16) to (19).

Table 1: Microgrid parameters [7,22,25]

Parameter	value	Parameter	value
$K_{DG}(s)$	1	$K_{FC}(s)$	1
$T_{DG}(s)$	2	$T_{FC}(s)$	4
$K_D(s)$	1	$K_{BESS}(s)$	1
$T_D(s)$	20	$T_{BESS}(s)$	0.1
$K_{AE}(s)$	1	$K_{FESS}(s)$	1
$T_{AE}(s)$	0.5	$T_{FESS}(s)$	0.1
$K_{SPV}(s)$	1	$K_{WTG}(s)$	1
$T_{SPV}(s)$	1.8	$T_{WTG}(s)$	0.5
M(pu s)	0.2	D(pu/Hz)	0.012

$$\begin{aligned} \dot{X} &= AX + BU \\ Y &= CX + DU \end{aligned} \quad (15)$$

$$A=\begin{bmatrix} \frac{-D}{2H} & 0 & \frac{1}{2H} & \frac{-1}{2H} & \frac{1}{2H} & \frac{1}{2H} & \frac{-1}{2H} & \frac{1}{2H} & \frac{1}{2H} \\ 0 & \frac{-1}{Tg} & 0 & 0 & 0 & 0 & 0 & 0 & 0 \\ 0 & \frac{1}{Tt} & \frac{-1}{Tt} & 0 & 0 & 0 & 0 & 0 & 0 \\ 0 & 0 & 0 & \frac{-1}{Tae} & 0 & 0 & 0 & 0 & 0 \\ 0 & 0 & 0 & 0 & \frac{-1}{Tfc} & 0 & 0 & 0 & 0 \\ 0 & 0 & 0 & 0 & 0 & \frac{-1}{T_{BESS}} & 0 & 0 & 0 \\ 0 & 0 & 0 & 0 & 0 & 0 & \frac{-1}{T_{FESS}} & 0 & 0 \\ 0 & 0 & 0 & 0 & 0 & 0 & 0 & \frac{-1}{T_{spv}} & 0 \\ 0 & 0 & 0 & 0 & 0 & 0 & 0 & 0 & \frac{-1}{T_{wtg}} \end{bmatrix} \quad (16)$$

$$B=\begin{bmatrix} 0 & 0 & 0 & \frac{-1}{2H} \\ \frac{1}{Tg} & 0 & 0 & 0 \\ 0 & 0 & 0 & 0 \\ \frac{1}{Tae} & 0 & 0 & 0 \\ \frac{1}{Tfc} & 0 & 0 & 0 \\ \frac{1}{T_{BESS}} & 0 & 0 & 0 \\ \frac{1}{T_{FESS}} & 0 & 0 & 0 \\ 0 & \frac{Kpv}{Tpv} & 0 & 0 \\ 0 & 0 & \frac{Kwtg}{Twtg} & 0 \end{bmatrix}, U=\begin{bmatrix} \Delta Pc \\ \Delta\phi \\ \Delta Pw \\ \Delta PL \end{bmatrix} \quad (17)$$

$$C=[-1\ \ 0\ \ 1\ \ -1\ \ 1\ \ 1\ \ -1\ \ 1\ \ 1], D=[0\ \ 0\ \ 0\ \ 1] \quad (18)$$

$$X=\begin{bmatrix} \Delta F \\ \Delta Pg \\ \Delta P_{deg} \\ \Delta Pae \\ \Delta Pfc \\ \Delta Pbess \\ \Delta Pfess \\ \Delta Pspv \\ \Delta Pwtg \end{bmatrix} \quad (19)$$

ΔP_{fess} : Power deviations of flywheel

ΔP_{spv} : Power deviations of Solar Photovoltaic

ΔP_{fc} : Power deviations of Fuel Cell

ΔP_{ae} : Aqua Electrolyzer

$\Delta\phi$: deviations of radiation

ΔP_{bess} : Power deviations of Battery

ΔF : Frequency deviations of microgrid

ΔP_{wtg} : Power deviations of Wind Turbine Generator

ΔP_w : Input power changes related to wind turbine

ΔP_L : Power deviations of Load

ΔP_g : Power deviations of governor

Using the geometric location diagram, the poles of the isolated microgrid are drawn. In Fig. 7-a, the poles of the microgrid are shown and in Fig. 7-b, the location of the poles of the microgrid is shown.

[DOR: 20.1001.1.23452951.1399.10.4.3.5]
[DOI: 10.22052.10.4.60]

[DOR: 20.1001.1.23452951.1399.10.4.3.5]

[DOI: 10.22052.10.4.60]

-10.0000+0.0001i: Flywheel Pole

-10.0000+0.0001i: Battery Pole

-6.6631+0.0000i: Pohtovoltaic Pole

-1.9969+0.0000i: Aqua Electrolyzer Pole

-0.6531+0.0000i: Wind Turbine Pole

-0.4998+0.0000i:Diesel Generator Pole

-0.2505+0.0000i: Fuel cell Pole

-0.0804+0.0000i: Rotating mass Pole

-0.0500+0.0000i:Diesel Generator Pole

Fig. 7-a: The microgrid poles

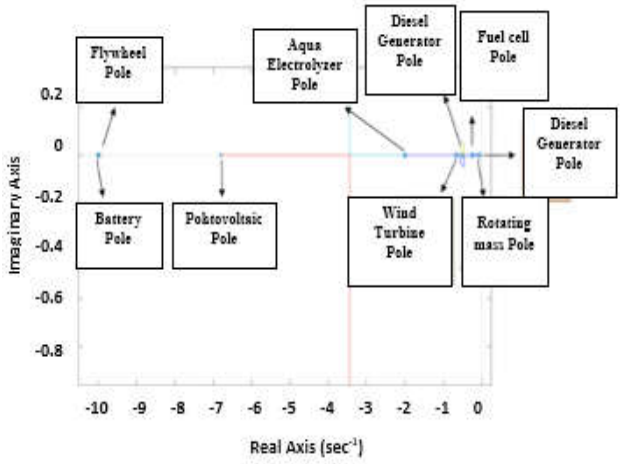

Fig. 7-b: The Location of microgrid poles

According to Fig. 7-a and Fig. 7-b, microgrid components can be divided into two groups of fast dynamic and slow dynamic. Solar cells are among the fast dynamic components. Wind turbine is among the slow dynamic components. Solar cell and wind turbine are among the uncontrollable components. Fast dynamic controllable components of the microgrid include the battery and flywheel. Slow dynamic controllable components of the microgrid include the diesel generator, electrolyzer, and fuel cell. In the proposed control strategy for fast dynamic controllable elements, a controller has been used which is, according to its fast dynamic, very effective in the transient state of the system. Therefore, the controller coefficients of these components are controlled so that the system can achieve a better transient state. Furthermore, the controller's coefficients of slow dynamic controllable components are controlled so that the system can have an optimal steady response.

4. Proposed Method

4. 1. Microgrid Classification Based on Dynamics

In the proposed method, at first, the controllable components of the microgrid are divided in two groups of fast dynamic and slow dynamic as shown in Fig. 8-a. Then, for the fast dynamic components of the microgrid, a fractional order proportional integral differential controller was used for more optimal control of the transient state as shown in Fig. 8-b. Following that, a fractional order proportional integral differential controller was used for the slow dynamic components, including: a diesel generator, a fuel cell, and electrolyzer, to control the steady states shown in Fig. 8-c. Following that, the parameters of two categories (slow and fast dynamic) were optimized using the Grey Wolf algorithm.

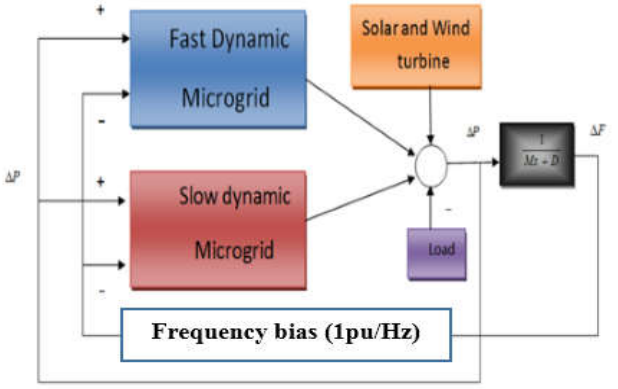

Fig. 8-a: Classification of controllable components of the microgrid into two fast and slow dynamic sections

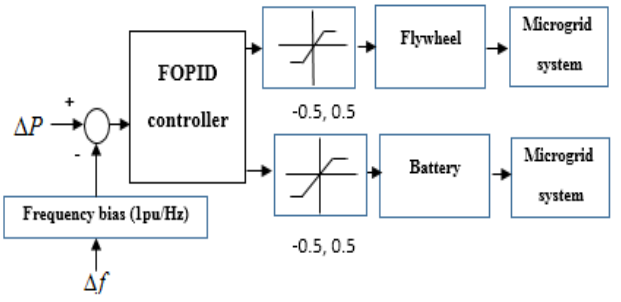

Fig. 8-b: Fast-dynamic components of the microgrid including battery and flywheel

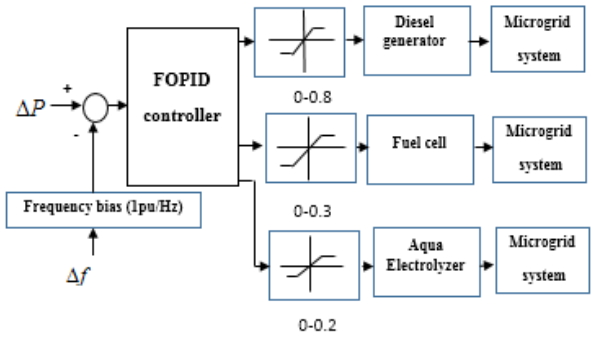

Fig. 8-c: slow-dynamic components of the microgrid including Diesel Generator, Aqua Electrolyzer and Fuel Cell

4. 2. Fractional Order Proportional Integral Differential Controller

The most common type of Proportional Integral Differential (PID) controller, i.e., the Fractional Order Proportional Integral Differential controller ($PI^{\lambda}D^{\mu}$), is the most common form of a fractional order controller. Equation (20) depicts the transfer function of the Fractional Order Proportional Integral Differential controller, which includes a proportional gain, an integral gain which is a λ stage integrator, and a differential gain which is of the μ stage ($\lambda,\mu>0$) [28,29].

By selecting $\lambda=1,\mu=1$ in the Fractional Order Proportional Integral Differential controller, a classic Proportional Integral Differential controller will be obtained. $\lambda=1,\mu=0$, and $\lambda=0,\mu=1$ are correspondent to conventional-Proportional-Integral and Proportional-Differential controllers respectively. All these classic types of Proportional-Integral-Differential controllers are the specific instances of the presented $PI^{\lambda}D^{\mu}$ controller (Fractional-Order-Proportional-Integral-Differential controller). The Fractional-Order-Proportional-Integral-Differential controller is an extension of the classic Proportional-Integral-Differential controller and expands it from the dot form to page form. Fig. 9 shows a Fractional-Order-Proportional-Integral-Differential controller [28,29].

$$G_c(s)=K_P+\frac{K_I}{S^{\lambda}}+K_D S^{\mu} \qquad (20)$$

One of the greatest advantages of the Fractional-Order-Proportional-Integral-Differential controller is better a control of dynamic systems. Another advantage of Fractional-Order-Proportional-Integral-Differential controllers is their less sensitive state to the parameter variations of a controlled system due to their two additional degrees of freedom for better regulation of the dynamic features of a fractional order control system.

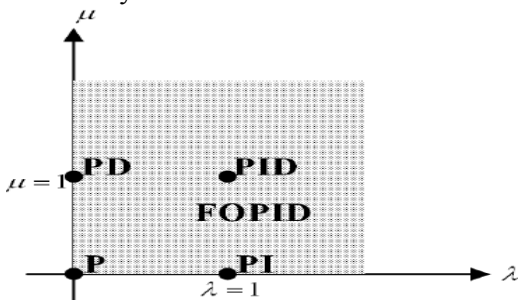

Fig. 9: FOPID controller [29]

4. 3. Grey Wolf Optimizer (GWO) Algorithm

Greys wolves are predators that mostly live in groups and have very precise group categorizations. The α wolf plays the role of the group leader at the top of this categorization, while w,δ,β wolves are in the next ranks. According to this categorization, each of the wolves has specific responsibilities. The more interesting fact about these wolves is their methods of hunting. After tracking and chasing their prey, they besiege it and attack it once that the prey was worn down. These hunting and grouping techniques of grey wolves have been implemented for optimizing the coefficients of Fractional-Order-Proportional-Integral-Differential controllers. In this optimizing algorithm, the best response in each repetition is considered as α, and the second and the third best responses are considered as β and δ respectively. Other responses are considered as w. Assuming that δ,β,α provide the best knowledge as to the potential location of the optimal response, the location of the other search agents (w) will, thus ,be updated based on the location of δ,β,α [30]. The Grey Wolf algorithm process is illustrated in Fig. 10.

4. 4. Optimizing the Fractional Order PID Controller via the Grey Wolf Algorithm for Controlling the Microgrid Load-Frequency

Equation (21) shows the objective function of the problem, and the constrained optimization problems are shown via (22).

$$\min J=\int_0^t t\left|\Delta f_1\right|^2 dt \qquad (21)$$

[DOR: 20.1001.1.23452951.1399.10.4.3.5]
[DOI: 10.22052.10.4.60]

J : The objective function
t: Simulation time
Δf_1 : Isolated microgrid frequency deviations

$$Kp_{\min} \le Kp \le Kp_{\max}$$
$$Ki_{\min} \le Ki \le Ki_{\max}$$
$$Kd_{\min} \le Kd \le Kd_{\max} \quad (22)$$
$$0 \le \lambda \le 1$$
$$0 \le \mu \le 1$$

The objective is to decrease microgrid frequency deviations through tan optimization of slow-dynamic and fast-dynamic controllers of the microgrid.

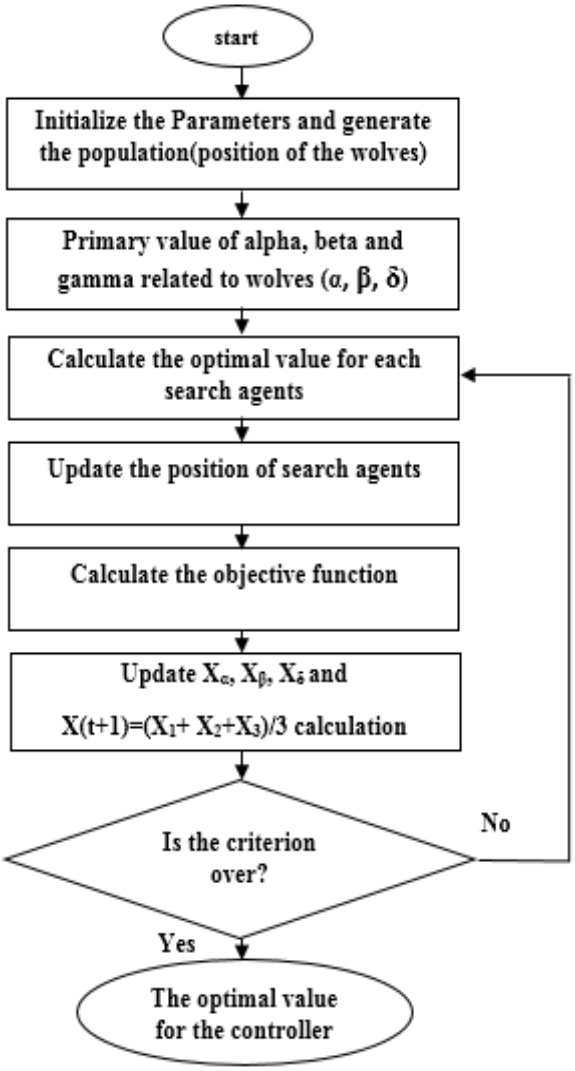

Fig. 10: The Flowchart for the Gray Wolf algorithm

The steps taken for the parameter optimization of Fractional-Order-Proportional-Integral-Differential controllers for controlling the load-frequency of the microgrid are as follows:

1. The initialization of Grey Wolf algorithm parameters (initial population value, the definition of the random value for r_1 and r_2 between the [0, 1] interval and the $\vec{a}$ vector which decreases from 2 to zero), boundary limits for search agents, and the initialization of the search agents or Grey Wolves (controlling parameters of Fractional-Order-Proportional-Integral-Differential controller which include ($K_P, K_i, K_d, \lambda, \mu$).

2. Calculating the objective function according to (21) and determining the α, β, δ wolves in the search area.

3. Updating the location of α, β, δ wolves.

4. Calculating $\vec{A}$ and $\vec{C}$ via $\vec{A} = 2\vec{a}\,\vec{r}_1 - \vec{a}, \vec{C} = 2\vec{r}_2$

5. Updating the location of search agents including ω using $\vec{X}_1 = \vec{X}_\alpha - \vec{A}_1(\vec{D}_\alpha), \vec{X}_2 = \vec{X}_\beta - \vec{A}_1(\vec{D}_\beta), \vec{D}_\alpha = \left|\vec{C}_1\vec{X}_\alpha - \vec{X}\right|, \vec{D}_\beta = \left|\vec{C}_2\vec{X}_\beta - \vec{X}\right|, \vec{D}_\delta = \left|\vec{C}_3\vec{X}_\delta - \vec{X}\right|$ equations, modifying the control variables ($K_P, K_i, K_d, \lambda, \mu$) for each search agent using the $X(t+1) = \frac{X_1(t) + X_2(t) + X_3(t)}{3}$ equation.

6. Investigating whether each search agent has gone beyond the search area or not and whether unsuitable solutions should be substituted by the set of produced random solutions.

7. Determining the location of search agents of the fifth step, from the best value to the worst value, and using it for the next generation.

8. Returning to the third step if repetitions have not ended.

5. Simulation

The value of microgrid parameters has been introduced in the section of microgrid components. An optimization of the J function has been performed in order to reduce the steady state error, to decrease the maximum overshoot, and to decrease the settling time caused by the state of load disturbances. Simulation has been performed using six different scenarios. In the first scenario, uncertainty has not been considered for microgrid parameters. In the second and the third scenarios, parameter uncertainty has been taken into account for the microgrid. In the fourth scenario, disturbances applied to the microgrid are considered as irregular pulse trains, and the results of the proposed method in all four scenarios have been compared with the conventional methods. In the

[DOR: 20.1001.1.23452951.1399.10.4.3.5]
[DOI: 10.22052.10.4.60]

fifth and sixth scenarios, the results of the proposed controller have been compared with the Fractional-Order-Proportional-Integral-Differential controller, the coefficients of which have been optimized using Particle Swarm and Genetic algorithms.

The initial parameters of the Grey Wolf algorithm and the constraints have been depicted in Table 2.

Table 2: Initial parameters and optimization constraints

Parameter	value
K_p	[0,3]
K_i	[0,3]
K_d	[0,3]
λ	[0,1]
μ	[0,1]
Grey wolf(GWO)	10
Iteration(GWO)	50
n_p	100

According to the data presented in Table 2, the Grey Wolf algorithm becomes convergent in all forms of simulations in fifty repetitions. Fig. 11 illustrates the convergence process of the Grey Wolf algorithm for scenario 1.

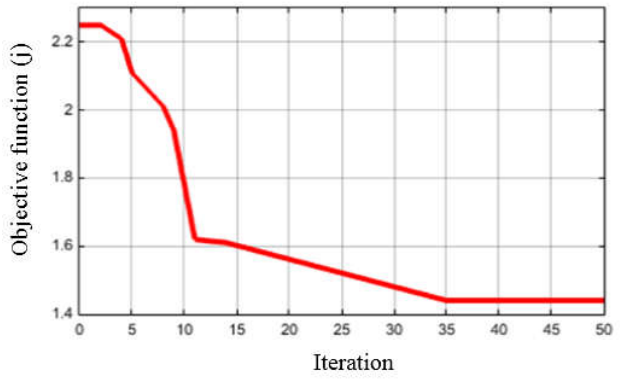

Fig. 11: The Convergence of the gray wolf algorithm for scenario 1

Scenario (1): Fig. 12 shows the load variations applied to the microgrid. Table 1 data have been used for the microgrid. Fig. 13 shows the frequency variations of the microgrid with regard to the disturbance variations applied to the microgrid using various controllers. The results of the proposed controller (Proportional-Integral-Differential controller, optimized via the Grey Wolf algorithm by categorizing the microgrid into two groups of slow and fast dynamic) have been compared with [1] and [7]. The performance of the proposed controller is more optimal in comparison with the Proportional-Integral-Differential controller, optimized using neural networks [1], and the Proportional-Integral-Differential controller, the coefficients of which have been obtained by the Ziegler-Nichols method. The coefficients of the proposed controllers (slow dynamic and fast dynamic) are outlined in Table 3 for scenario (1). Table 4 shows the controllers' performance results for scenario (1).

Scenario (2): Fig. 12 illustrates the disturbances applied to the microgrid. In this scenario, uncertainty has been considered for the microgrid parameters so that the inertia constant varies between the range of [0.5 1]. Table 1 data have been used. Fig. 14 shows frequency variations of the microgrid with respect to the disturbances applied to the microgrid, according to Fig. 12, using various controllers. The results of the proposed controller have been compared with [1] and [7]. The performance of the proposed controller against uncertainty of the parameters is more optimal in comparison with the Proportional-Integral-Differential controller, optimized using neural networks [1], and the Proportional-Integral-Differential controller, the coefficients of which have been obtained by the Ziegler-Nichols method. Table 5 shows the results of various controllers for scenario (2).

Scenario (3): Fig. 12 illustrates the disturbances applied to the microgrid. In this scenario, uncertainty has been considered for the microgrid parameters so that the inertia constant varies between the range of [1 1.5]. Table 1 data have been used. Fig. 15 shows the frequency variations of the microgrid with respect to the disturbances applied to the microgrid, according to Fig. 12, using various controllers. The results of the proposed controller have been compared with [1] and [7]. The performance of the proposed controller against uncertainty of the parameters is more optimal in comparison with the Proportional Integral Differential controller, optimized using neural networks [1], and the Proportional Integral Differential controller, the coefficients of which have been obtained by the Ziegler-Nichols method. Table 6 shows the results of various controllers for scenario (3).

Scenario (4): In this scenario, load disturbances are applied to the microgrid as irregular pulse trains

[DOR: 20.1001.1.23452951.1399.10.4.3.5]
[DOI: 10.22052.10.4.60]

as shown in Figure 16. Table 1 data have been used. Fig. 17 shows the frequency variations of the microgrid with respect to the disturbances applied to the microgrid, according to Fig. 16, using various controllers. The results indicate that the performance of the proposed controller against intense load variations is more optimal in comparison with the Proportional-Integral controller, optimized using neural networks, and the Proportional-Integral-Differential controller, the coefficients of which have been obtained by the Ziegler-Nichols method. Table 7 shows the results of various controllers for scenario (4).

Scenario (5): This scenario has been presented to compare the control method (the Fractional-Order-Proportional-Integral-Differential controller, optimized via the Grey Wolf algorithm) with the Fractional-Order-Proportional-Integral-Differential controller that has been optimized using the particle swarm algorithm and the genetic algorithm. Load disturbances have been applied to the microgrid as shown in Fig. 18. Table 1 data have been used. Fig. 19 shows the frequency variations of the with respect to load disturbances using various controllers. According to Fig. 19, the performance of the proposed control method is more optimal compared with the Fractional-Order-Proportional-Integral-Differential controller using particle swarm algorithm and genetic algorithm.

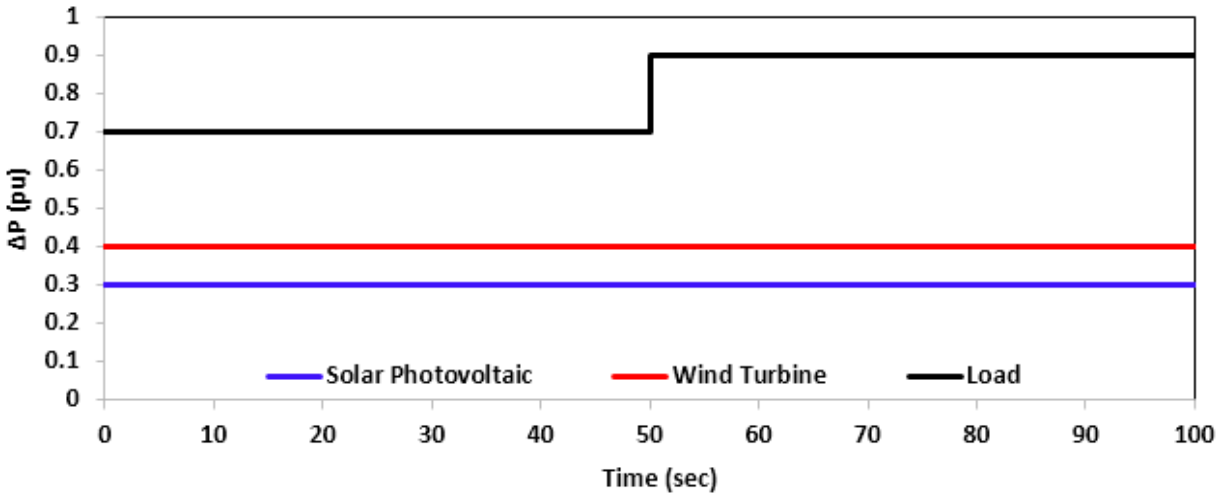

Fig. 12: The Disturbance on the microgrid [7]

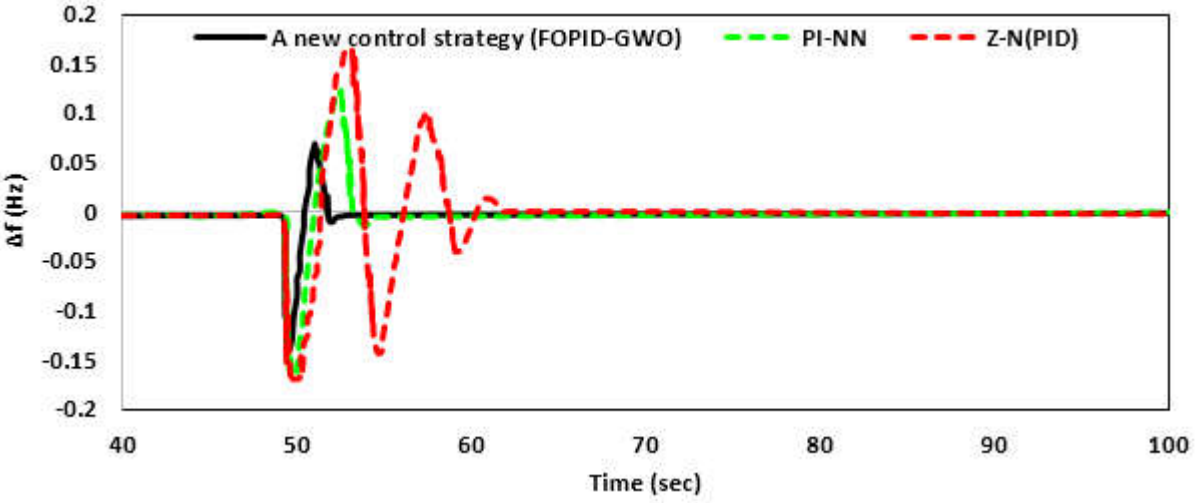

Fig. 13: The Frequency response of the microgrid due to load disturbances using different control methods

[DOR: 20.1001.1.23452951.1399.10.4.3.5]
[DOI: 10.22052.10.4.60]

Table 3: FOPID controller coefficients for both fast dynamic and slow dynamic sections

Microgrid sections that have dynamic and fast dynamics	FOPID controller coefficients of fast and dynamic dynamics section (coefficients optimized by gray wolf)				
	K_P	K_i	K_d	λ	μ
New control strategy using FOPID –GWO, controller fast dynamics control factor (battery and flywheel)	0.465	0.1056	1.0286	0.867	0.982
New control strategy using FOPID –GWO, controller slow dynamics control factor (Diesel generator, fuel cell and electrolyzer)	0.0465	0.1112	1.0384	0.897	0.982

Table 4: settling time, peak overshoot and peak undershoot using different controllers

Scenario (1)	$\Delta f\,(Hz)$		
Control method	peak overshoot	peak undershoot	settling time (sec)
A new control strategy (GWO-FOPID)	0.07	-0.14	5.67
PI-NN	0.12	-0.17	6.96
Z-N PID	0.18	-0.17	12.43

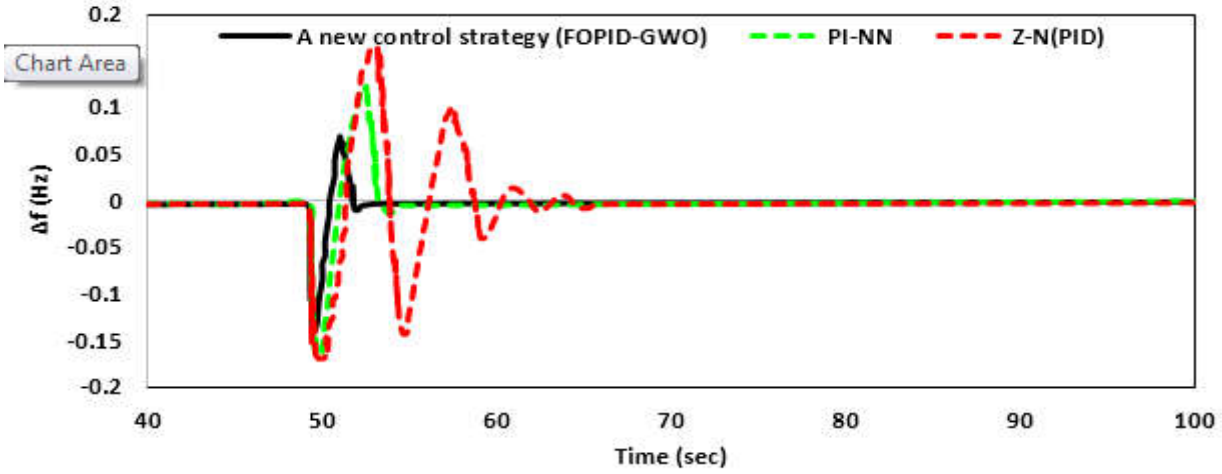

Fig. 14: The Frequency response of the uncertainty of the microgrid parameters, Scenario 2

Table 5: settling time, peak overshoot and peak undershoot using different controllers, , Scenario 2

Scenario (2)	$\Delta f\,(Hz)$		
Control method	peak overshoot	peak undershoot	settling time (sec)
A new control strategy(GWO-FOPID)	0.065	-0.134	5.02
PI-NN	0.12	-0.161	6.21
Z-N PID	0.18	-0.165	14.24

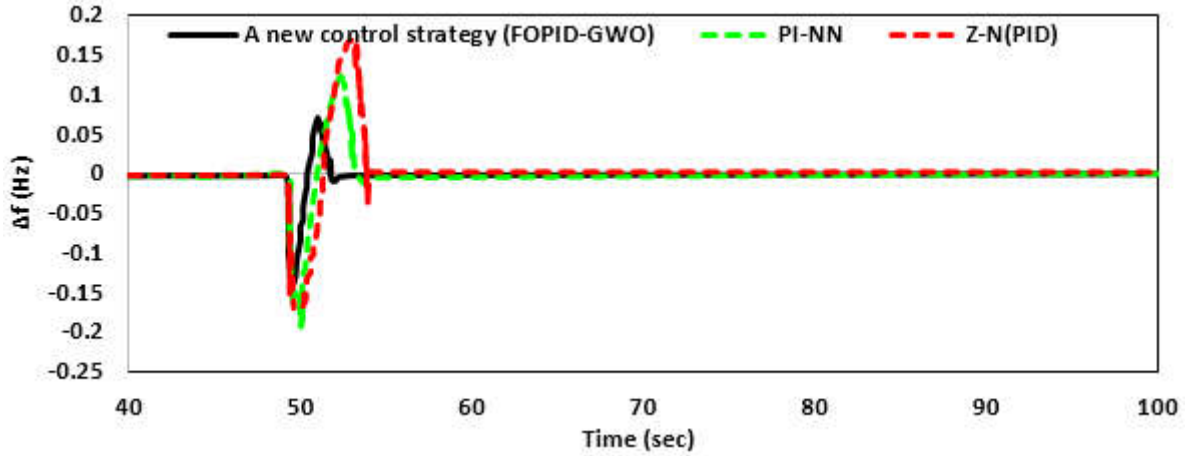

Fig. 15: The Frequency response of the uncertainty of the microgrid parameters, Scenario 3

Table 6: settling time, peak overshoot and peak undershoot using different controllers, , Scenario 3

Scenario (3)	$\Delta f\ (Hz)$		
Control method	peak overshoot	peak undershoot	settling time (sec)
A new control strategy(GWO-FOPID)	0.052	-0.124	4.83
PI-NN	0.14	-0.191	5.41
Z-N PID	0.18	-0.1486	6.32

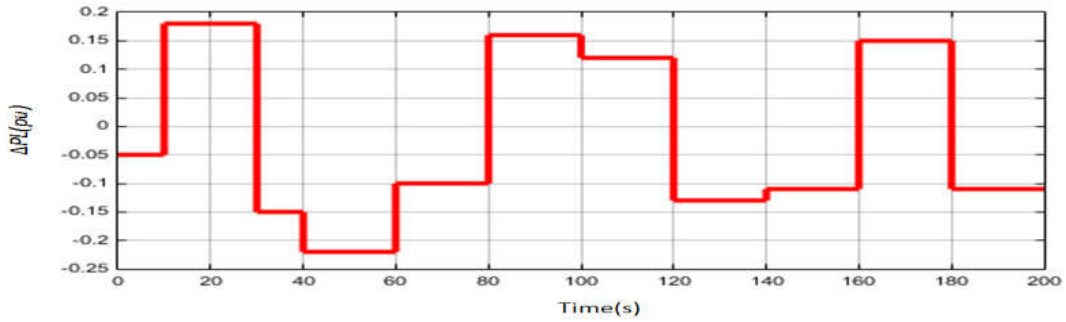

Fig. 16: The load disturbances

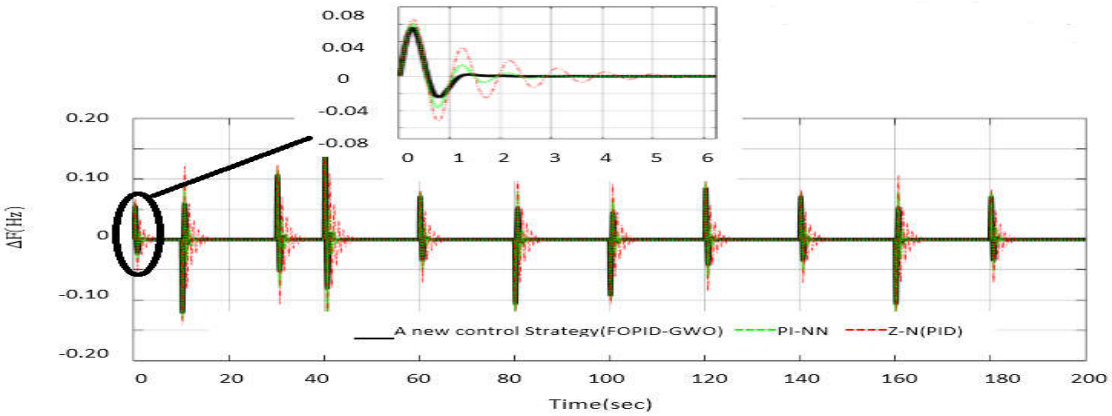

Fig. 17: The Frequency response of the microgrid

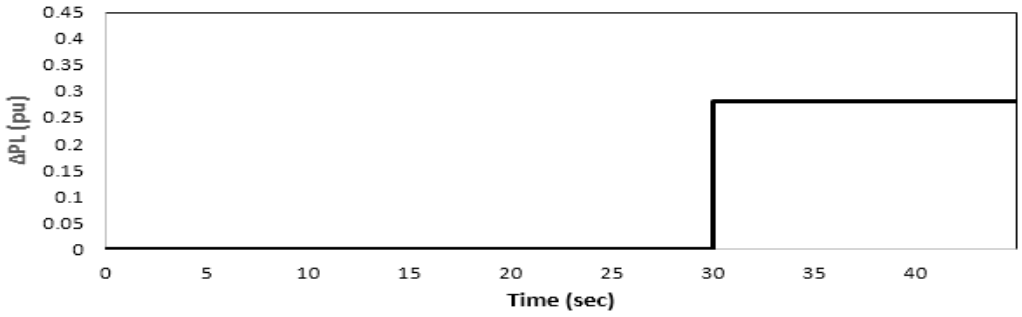

Fig. 18: The load disturbances, Scenario 5

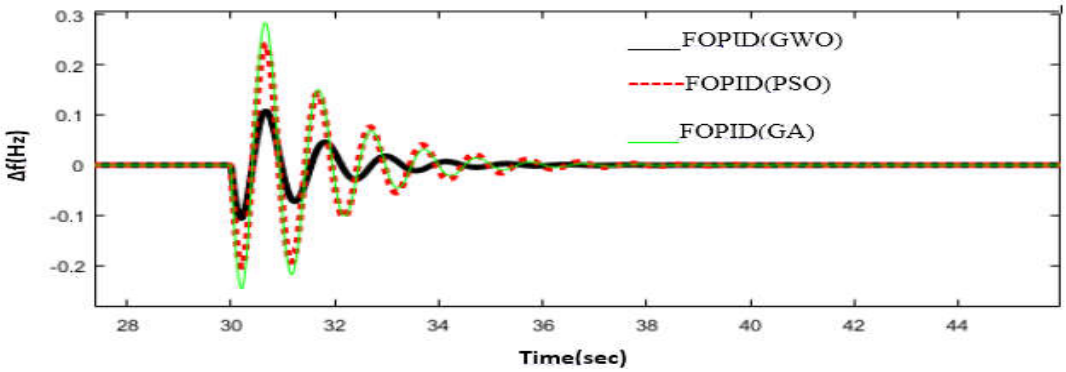

Fig. 19: The Frequency response of the microgrid, Scenario 5

[DOR: 20.1001.1.23452951.1399.10.4.3.5]
[DOI: 10.22052.10.4.60]

Scenario (6): In this scenario, according to Fig. 20, the load disturbances are applied as a step to the microgrid. Fig. 21 shows the frequency changes of the microgrid to load disturbances using different controllers. According to Fig. 21, the performance of the proposed control method is more optimal compared with the Fractional-Order-Proportional-Integral-Differential controller using particle swarm algorithm and genetic algorithm.

6. Conclusion

In this paper, microgrids are firstly categorized into two groups of slow dynamic and fast dynamic, based on the linear model of microgrid components. Since the fast dynamic components are extremely influential on the transient state of the system, transient states superior to the conventional control strategies can be achieved by optimizing the controlling parameters of the fast dynamic components, and optimal steady states can be obtained by optimizing the controlling parameters of the slow dynamic components. The Fractional-Order-Proportional-Integral-Differential controller, optimized using the Grey Algorithm, has been used as the controller for controllable microgrid components. As simulation results show, the proposed control strategy has optimal performance in comparison with the conventional methods (PID and PI, the coefficients of which have been optimized using the Ziegler-Nichols and neural network methods respectively), as well as the Fractional Order Proportional Integral Differential controller (FOPID) which has been optimized using particle swarm and genetic algorithms.

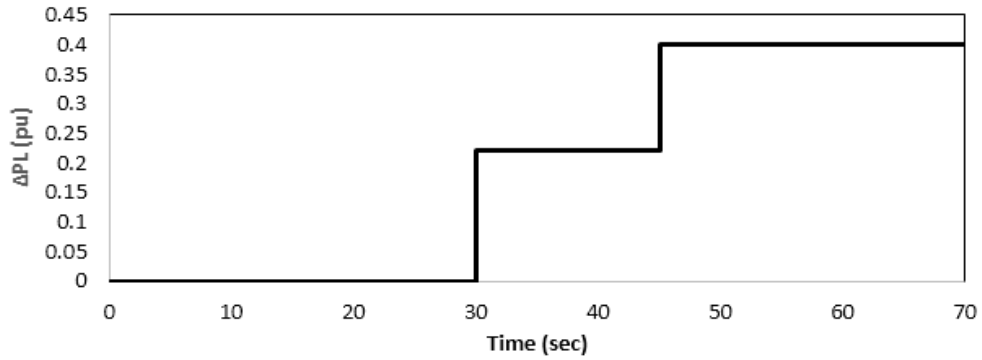

Fig. 20: The load disturbances, Scenario 6

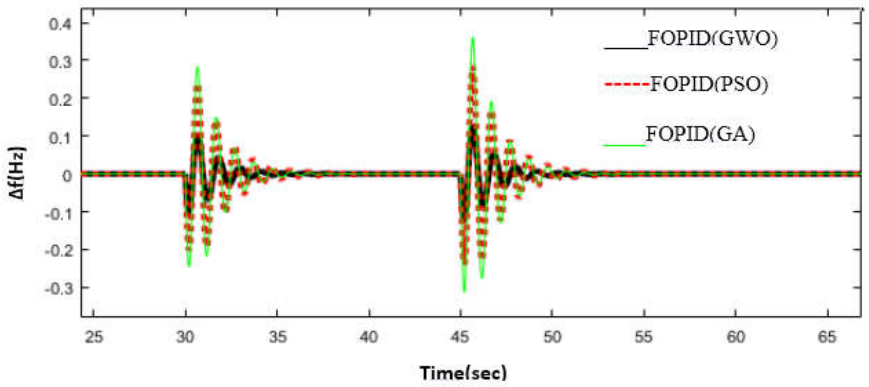

Fig. 21: The Frequency response of the microgrid, Scenario 6

References

[1] Habibi, F., Bevrani, H. and Moshtagh. J., "*The Use of Artificial Neural Networks in the Design of a Smart Frequency Controller for An Islanded Microgrid*", Iranian Journal of Electrical and Computer Engineering, Vol. 10, No. 2, pp. 88-96, 2012.

[2] Hajiaghasi, S. and Salemnia, Hamzeh M., "*A New Method for Determination of Hybrid Energy Storage Capacity in Isolated Microgrid*", Energy Engineering & Management, Vol. 9, No. 3, pp. 50-63, 2019.

[3] Shahgholian, G., Fani, B., Keyvani, B., Karimi, H. and Moazzami, M., "*An Improvement in the Reactive Power Sharing by the Use of Modified Droop Characteristics in*

Autonomous Microgrids", Energy Engineering & Management, Vol. 9, No. 3, pp. 64-71, 2019.

[4] Amiri, F. and Hatami, A., "*A Model Predictive Control Method for Load-Frequency Control in Islanded Microgrids*", Computational Intelligence in Electrical Engineering, Vol. 8, No. 1, pp. 9-24. 2017.

[5] Amraee, T., Ranjbar, A. and Mozaffari, B., "*Multi-Stage Under Frequency Load Shedding Relay in Islanded Distribution Systems*", Energy Engineering & Management, Vol. 7, No. 4, pp. 2-11, 2018.

[6] Shahbazi, M. and Amiri, F., "*Designing a Neuro-Fuzzy Controller with CRPSO and RLSE Algorithms to Control Voltage and Frequency in An Isolated Microgrid*", In 2019 International Power System Conference (PSC). IEEE, pp. 588-594, IEEE, 2019.

[7] Mallesham, G., Mishra, S., Member, S. and Jha, A. N., "*Ziegler-Nichols Based Controller Parameters Tuning for Load Frequency Control in A Microgrid*", in Proceedings of the IEEE International Conference on Energy, Automation, and Signal, pp.1-8, 2011.

[8] Das, D. C., Roy, A. K. and Sinha, N., "*PSO based Frequency Controller for Wind- Solar-Diesel Hybrid Energy Generation /Energy Storage System*", in Proceedings of the IEEE International Conference on Energy, Automation, and Signal, pp. 1-6. 2011,

[9] Li, J. M. and Li, P., "Research on Microgrid Frequency Control with Droop Characteristic Based on Lagrange Interpolation", In *Applied Mechanics and Materials*, Vol. 556, pp. 1814-1817, 2014.

[10] Tidjani, F. S., Hamadi, A., Chandra, A., Pillay, P. and Ndtoungou, N., "*Optimization of Standalone Microgrid Considering Active Damping Technique and Smart Power Management using Fuzzy Logic Supervisor*", IEEE Transactions on Smart Grid, Vol. 8, No. 1, pp. 475-484, 2017.

[11] Masui, K., Takamura, S. and Namerikawa, T., "*Load Frequency Control of a Microgrid Based on H∞ Control Considering Response Speed of Generators*", Transactions of the Society of Instrument and Control Engineers, Vol. 51, pp. 570-578, 2015.

[12] Singh, V. P., Mohanty, S. R., Kishor, N. and Ray, P. K., "*Robust H-infinity Load Frequency Control in Hybrid Distributed Generation System*", Int J. Electr. Power Energy System, Vol. 46, pp. 294-305, 2013.

[13] Azizi, S. M. and Khajehoddin, S. A., "*Robust Load Frequency Control in Islanded Microgrid Systems using μ-Synthesis and D-K Iteration*", 2016 Annual IEEE Systems Conference (SysCon), Orlando, FL, pp. 1-8, 2016

[14] Amiri, F. and Moradi, M. H., "*Designing a Fractional Order PID Controller for a Two-Area Micro-Grid under Uncertainty of Parameters*", Iranian Journal of Energy, Vol. 20, No. 4, pp. 49-78, 2018.

[15] Shafiee, Q., Guerrero, J. M. and Vasquez, J. C., "*Distributed Secondary Control for Islanded Microgrid –A Novel Approach*", IEEE Transactions on Power Electronics, Vol. 29, No. 2, pp. 1018-1031. 2014.

[16] Elrayyah, A., Cingoz, F. and Sozer, Y., "*Smart Loads Management using Droop-Based Control in Integrated Microgrid Systems*", IEEE Journal of Emerging and Selected Topics in Power Electronics, Vol. 5, No. 3, pp. 1142-1153, 2017.

[17] Cingoz, F., Elrayyah, A. and Sozer, Y., "*Plug-and-Play Nonlinear Droop Construction Scheme to Optimize Islanded Microgrid Operations*", IEEE Transactions on Power Electronics, Vol. 32, No. 4, pp. 2743-2756, 2017.

[18] Rana, R., Singh, M. and Mishra, S., "*Design of Modified Droop Controller for Frequency Support in Microgrid using Fleet of Electric Vehicles*", IEEE Transactions on Power Systems, Vol. 32, No. 5, pp. 3627-3636, 2017.

[19] Mu, C., Tang, Y. and He, H., "*Observer-based Sliding Mode Frequency Control for Microgrid with Photovoltaic Energy Integration*", 2016 IEEE Power and Energy Society General Meeting (PESGM), Boston, MA, pp. 1-5, 2016.

[20] Das, D. C., Roy, A. K. and Sinha, N., "*GA based Frequency Controller for Solar Thermal–Diesel–Wind Hybrid Energy Generation/Energy Storage System*", Int J. Electr. Power Energy System, Vol. 43, No. 1, pp. 262–279, 2012.

[21] Pandey, S. K., Mohanty, S. R, Kishor, N. and Catalão, J. P. S., "*Frequency Regulation in Hybrid Power Systems using Particle Swarm Optimization and Linear Matrix Inequalities based Robust Controller Design*", Int J. Electr. Power Energy System, Vol. 63, pp. 887–900, 2014.

[22] El-Fergany, A. A. and El-Hameed, M. A., "*Efficient Frequency Controllers for Autonomous Two-Area Hybrid Microgrid System using Social-Spider Optimizer*", IET Generation, Transmission & Distribution, Vol. 11, No. 3, pp. 637-648, 2017.

[23] Kumar, R. H. and Ushakumari, S., "*Biogeography-based Tuning of PID Controllers for Load Frequency Control in Microgrid*", 2014 International Conference on Circuit, Power and Computing Technologies [ICCPCT], Nagercoil, pp. 797-802, 2014.

[24] Shankar, G. and Mukherjee, V., "*Load Frequency Control of an Autonomous Hybrid Power System by Quasi-Oppositional Harmony Search Algorithm*", *Int J. Electr. Power Energy Syst*em, Vol. 78, pp. 715–734, 2016.

[25] Bevrani, H., Habibi, F., Babahajyani, P., Watanabe, M. and Mitani, Y., "*Intelligent Frequency Control in An Ac Microgrid: Online PSO-based Fuzzy Tuning Approach*", IEEE Transactions on Smart Grid, Vol. 3, No. 4, pp. 1935-1944, Dec. 2012.

[26] Amiri, F. and Hatami, A., "*Load Frequency Control Via Adaptive Fuzzy PID Controller In An Isolated Microgrid*", In 32nd International Power System Conference, 2017.

[27] Khooban, M. H., Niknam, T., Blaabjerg, F., Davari, P. and Dragicevic, T., "*A New Load Frequency Control Strategy for Micro-grids with Considering Electrical Vehicles*", Electric Power Systems Research, Vol. 143, pp. 585-598, 2017.

[28] Amiri, F. and Hatami, A., "*Nonlinear Load Frequency Control of Isolated Microgrid using Fractional Order PID based on Hybrid Craziness-based Particle Swarm Optimization and Pattern Search*", Journal of Iranian Association of Electrical and Electronics Engineers, Vol. 17, No.2, pp. 135-148, 2020.

[29] Seo, S. W. and Choi, H. H., "*Digital Implementation of Fractional Order PID-Type Controller for Boost DC–DC Converter*", IEEE Access, Vol. 7, pp. 142652-142662, 2019.

[30] Alomoush, A. A., Alsewari, A. A., Alamri, H. S., Aloufi, K. and Zamli, K. Z. "*Hybrid Harmony Search Algorithm with Grey Wolf Optimizer and Modified Opposition-based Learning*", IEEE Access, Vol. 7, pp. 68764-68785, 2019.

[31] Gupta, E. and Saxena, A., "*Robust Generation Control Strategy based on Grey Wolf Optimizer*", Journal of Electrical Systems, Vol. 11, No. 2, pp. 174-188, 2015.

[DOR: 20.1001.1.23452951.1399.10.4.3.5]

[DOI: 10.22052.10.4.60]